

## ii 25. *Particle detectors*

### PARTICLE DETECTORS

To reduce the size of this section's PostScript file, we have divided it into three PostScript files. We present the following index:

#### PART 1

---

Page #	Section name
1	25.1 Organic scintillators—by K. Johnson (FSU)
5	25.2 Inorganic scintillators—by C.L. Woody (BNL)
5	25.3 Čerenkov detectors—by D.G. Coyne (UCSC)
8	25.4 Transition radiation detectors (TRD's)—by D. Froidevaux (CERN)
10	25.5 Silicon photodiodes and particle detectors—by H.F.W. Sadrozinski (UCSC) and H.G. Spieler (LBNL)
11	25.6 Proportional and drift chambers

---

---

#### PART 2

---

Page #	Section name
13	25.7 Time-projection chambers—by M.T. Ronan (LBNL)

---

---

#### PART 3

---

Page #	Section name
16	25.8 Calorimeters
18	25.9 Measurement of particle momenta in a uniform magnetic field
20	25.10 Superconducting solenoids for collider detectors by R.D. Kephart (FNAL)
22	25.11 Other observations
22	References

---

---

## 25.7. Time-projection chambers

Written November 1997 by M.T. Ronan (LBNL).

Detectors with long drift distances perpendicular to a multi-anode proportional plane provide three-dimensional information, with one being the time projection. A (typically strong) magnetic field parallel to the drift direction suppresses transverse diffusion ( $\sigma = \sqrt{2Dt}$ ) by a factor

$$D(B)/D(0) = \frac{1}{1 + \omega^2\tau^2}, \quad (25.14)$$

where  $D$  is the diffusion coefficient,  $\omega = eB/mc$  is the cyclotron frequency, and  $\tau$  is the mean time between collisions. Multiple measurements of  $dE/dx$  along the particle trajectory combined with the measurement of momentum in the magnetic field allows excellent particle identification [48], as can be seen in Fig. 25.3.

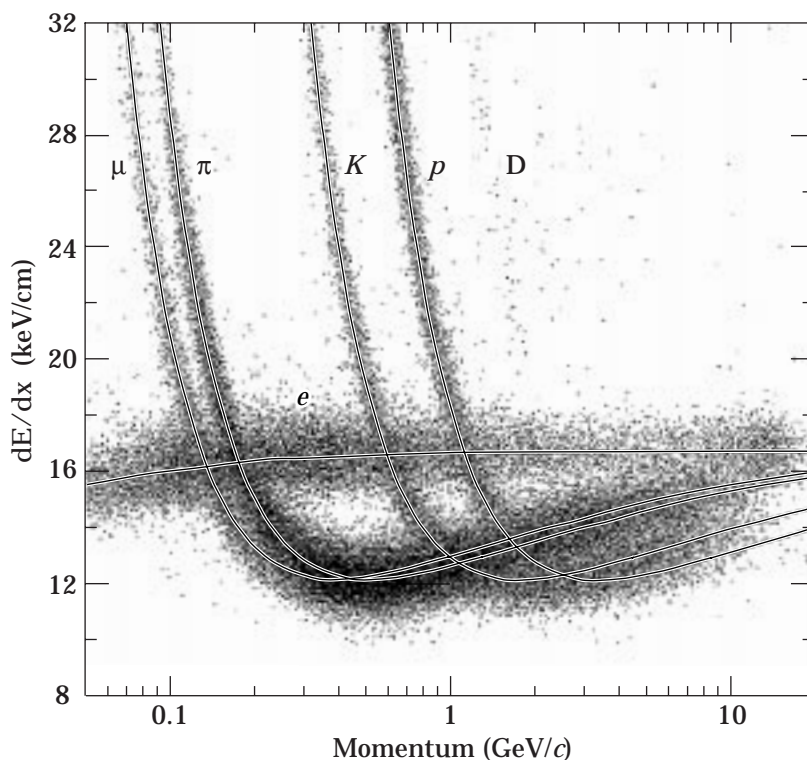


**Figure 25.3:** PEP4/9-TPC  $dE/dx$  measurements (185 samples @8.5 atm Ar-CH<sub>4</sub> 80–20%) in multihadron events. The electrons reach a Fermi plateau value of 1.4 times minimum. Muons from pion decays are separated from pions at low momentum;  $\pi/K$  are separated over all momenta except in the cross-over region. (Low-momentum protons and deuterons originate from hadron-nucleus collisions in inner materials such as the beam pipe.)

## 14 25. Particle detectors

A typical gas-filled TPC consists of a long uniform drift region (1–2 m) generated by a central high-voltage membrane and precision concentric cylindrical field cages within a uniform, parallel magnetic field [49]. Details of construction and electron trajectories near the anode end are shown in Fig. 25.4. Signal shaping and processing using analog storage devices or FADC's allows excellent pattern recognition, track reconstruction, and particle identification within the same detector.

Typical values:

$$\text{Gas: Ar + (10–20\%) CH}_4 \quad \text{Pressure}(P) = 1\text{--}8.5 \text{ atm.}$$

$$E/P = 100\text{--}200 \text{ V/cm/atm} \quad B = 1\text{--}1.5 \text{ Tesla}$$

$$v_{\text{drift}} = 5\text{--}7 \text{ cm}/\mu\text{s} \quad \omega\tau = 1\text{--}8$$

$$\sigma_{x \text{ or } y} = 100\text{--}200 \mu\text{m} \quad \sigma_z = 0.2\text{--}1 \text{ mm}$$

$$\sigma_{dE/dx} = 2.5\text{--}5.5 \%$$

Truncated mean  $dE/dx$  resolution depends on the number and size of samples, and gas pressure:

$$\sigma_{dE/dx} \propto N^{-0.43} \times (P\ell)^{-0.32} . \quad (25.15)$$

Here  $N$  is the number of samples,  $\ell$  is the sample size, and  $P$  is the pressure. Typical  $dE/dx$  distributions are shown in Fig. 25.3. Good three-dimensional two-track resolutions of about 1–1.5 cm are routinely achieved.

$E \times B$  distortions arise from nonparallel  $E$  and  $B$  fields (see Eq. 2.6 in Ref. 49), and from the curved drift of electrons to the anode wires in the amplification region. Position measurement errors include contributions from the anode-cathode geometry, the track crossing angle ( $\alpha$ ),  $E \times B$  distortions, and from the drift diffusion of electrons

$$\sigma_{x \text{ or } y}^2 = \sigma_0^2 + \sigma_D^2(1 + \tan^2 \alpha)L/L_{\text{max}} + \sigma_\alpha^2(\tan \alpha - \tan \psi)^2 \quad (25.16)$$

where  $\sigma$  is the coordinate resolution,  $\sigma_0$  includes the anode-cathode geometry contribution,  $\psi$  is the Lorentz angle, and  $L$  is the drift distance.

Space-charge distortions arise in high-rate environments, especially for low values of  $\omega\tau$ . However, they are mitigated by an effective gating grid (Fig. 25.4). Field uniformities of

$$\int (E_\perp/E) dz \lesssim 0.5\text{--}1 \text{ mm} , \quad (25.17)$$

over 10–40 m<sup>3</sup> volumes have been obtained. Laser tracks and calibration events allow mapping of any remnant drift non-uniformities.

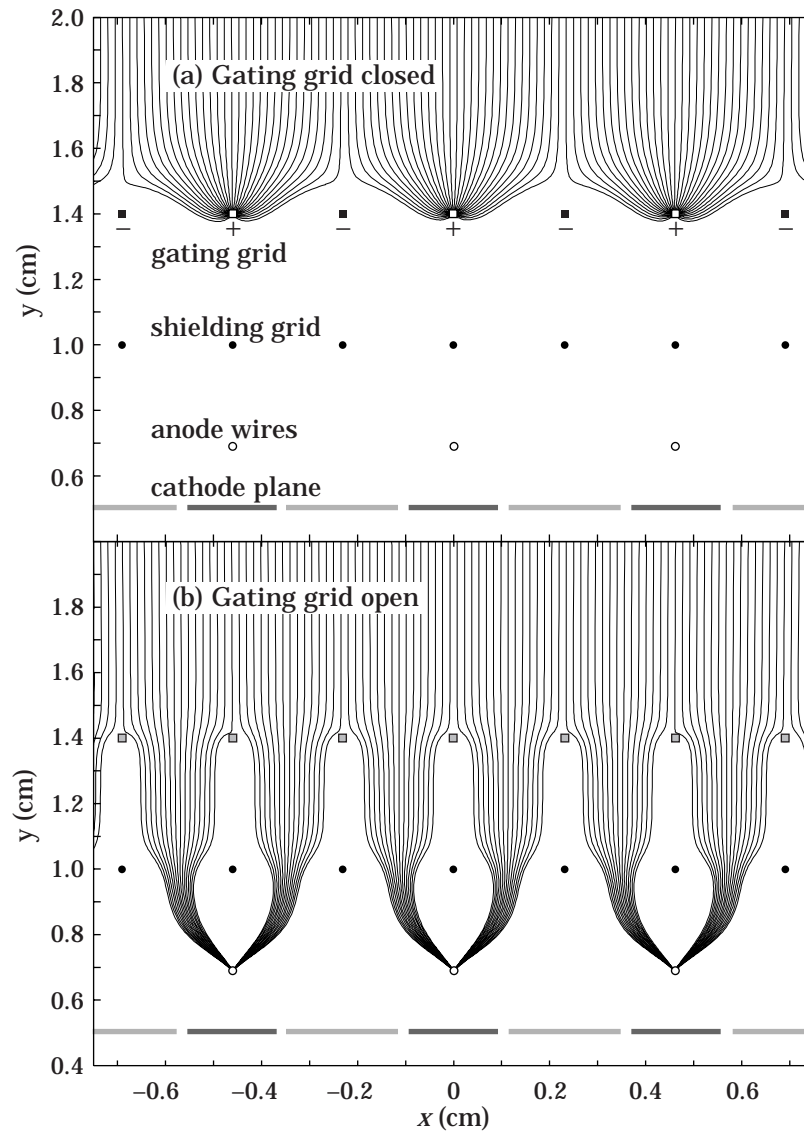


**Figure 25.4:** (a) Drifting electrons are collected on the gating grid until gated open by a triggering event. A shielding grid at ground potential is used to terminate the drift region. Electrons drifting through an open gating grid (b) pass through to the amplification region around the anode wires. Positive ions generated in the avalanche are detected on segmented cathode pads to provide precise measurements along the wire. The slow positive ions are blocked from entering the drift region by closing the gating grid after the electrons have drifted through.